THE JOURNAL OF PHYSICAL CHEMISTRY LETTERS
A JOURNAL OF THE AMERICAN CHEMICAL SOCIETY

pubs.acs.org/JPCL

Letter

Anomalous Water Wetting on a Hydrophilic Substrate under a High Electric Field

Qiuhao Xu,[#] Yutian Shen,[#] Cui Zhang,* Runlai Xu, Qunfang Gu, Haizhong Guo,* and Sheng Meng*

Cite This: *J. Phys. Chem. Lett.* 2023, 14, 11735−11741

Read Online

ACCESS | Metrics & More | Article Recommendations

ABSTRACT: Macroscopically, the traditional Young−Lippmann equation is used to describe the water contact angle under a weak electric field. Here we report a new wetting mechanism of deionized water under a strong electric field that defies the conventional Young−Lippmann equation. The contact angle of the deionized water droplet on a model hexagonal lattice with a different initial wettability is extensively modulated by the vertical electric field. The cosine of water contact angle on a hydrophilic substrate displays an anomalous linear relationship with the field, in contrast to the hydrophobic case, which shows an inverse parabolic relationship. Such anomalous wetting is verified by experimental measurements of water droplets on a pyroelectric substrate. Moreover, we identify that this anomaly arises from the linear modulation of the solid−liquid interfacial tension of hydrophilic substrates by the electric field. Our findings provide atomistic insight into the fundamental laws and new phenomena of water-surface interactions under extreme electric fields.

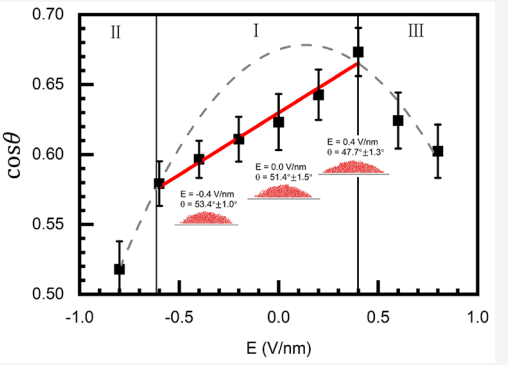

Interfaces play a central role in water science.[1−5] Understanding the interactions between water and the substrate at the atomic level is essential for controlling processes such as self-cleaning, lubrication, corrosion, as well as chemical reactions.[6−9] Various methods have been developed to manipulate the properties of water near the interface, including surface polarization or modification, microstructuring, and chemical modifications.[10−12]

In particular, electrowetting[13] and electrofreezing,[14] which use the external electric field or surface charges to control the wetting state of water, have long attracted extensive attention. In this regard, some previous studies have focused on the effects of the electric field or surface charges on the molecular structure of bulk water. For example, Svishchev et al.[15] found that the bulk sample of liquid water with a suitable density can freeze into cubic ice when subjected to a homogeneous static electric field; however, liquid water with other densities will transform into amorphous ice. Many other studies have focused on the impact of an electric field on interfacial water.[16] Yan et al.[17] showed that a local electric field parallel to the interface and acting only near the interface plays a major role in the nucleation of heterogeneous ice. Zhu et al.[18] demonstrated that the water overlayer on charged graphene undergoes first-order ice-to-liquid and then liquid-to-ice phase transitions with the increase of charge densities. In addition, there are also research advances in the influence of the electric field environment on water droplets.[19] In an external electric field, water molecules prefer to align their dipoles along the direction of the field, so the behaviors of water droplets will change at the atomic level to minimize the total energy. Kargar et al.[20] found that the nanodroplets elongate in the field direction when the amplitude of the applied field is larger than 0.8 V/nm, where the threshold of field will increase under the influence of a gigahertz electric field. Recently, the wetting ability on several polarized solid surfaces has also been investigated. Surblys et al.[11] found that the polarization direction of substrate affects the structures of the adsorbed layer and the rotational mobility of water. Bistafa et al.[12] investigated the water droplets on hydroxylated silica surfaces and pointed out that an increase of hydroxyl density improves the wettability due to interfacial entropy loss.

In the usual experimental setup for electrowetting on the dielectric (EWOD),[21] a conducting water droplet spreads out under a weak electric field, and the ions in water lead to an electrical "double layer" at the interface, restricting the field at the bottom of the droplet. When the size of droplet is well below the Debye shielding length, or there are not enough ions to form a double layer to shield the strong electric field (e.g., the deionized water), formulas such as the conventional Young−Lippmann equation, describing the water contact

Received: November 5, 2023
Revised: December 14, 2023
Accepted: December 15, 2023
Published: December 19, 2023

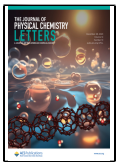

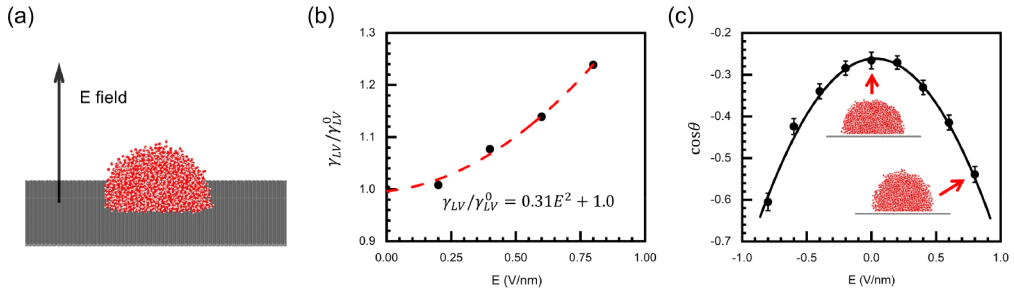

Figure 1. (a) Schematic diagram for a water droplet on the model hexagonal (0001) facet under a vertical electric field. (b) Nonlinear variation of the relative surface tension of water droplets on a hydrophobic substrate with electric field, obtained by MD simulations. Here the gas atmosphere is simplified to a vacuum, and γ_{LV}^0 represents the surface tension of liquid water without an electric field. (c) Parabolic relationship between the cosine of WCA and the external electric field strength on a hydrophobic substrate. The insets show snapshots of the side view of the water droplet.

angle (WCA) of droplets in an electric field under the assumption of double layer formation near the interface, are not expected to be suitable. Therefore, a systematic study of the atomic-scale wettability of deionized water in an electric field is urgently needed.

In this work, the characteristics of WCA on a solid substrate and the molecular structure of deionized water at the interface under the influence of a static vertical electric field are investigated by combining atomistic molecular dynamics (MD) simulations and experimental approaches. It is found that when the interaction between the substrate and water droplet is weak, i.e., on the hydrophobic substrate, regardless of the direction of the electric field applied (upward or downward along the surface normal direction), the WCA will increase as the field strength increases. However, on the hydrophilic substrates, the WCA exhibits anomalous behavior, decreasing in the gradually increasing upward electric fields but showing the opposite in the downward electric fields. Also, this peculiar wetting behavior is corroborated by experimental observations of water droplets on a pyroelectric substrate at abrupt temperature jumps. Our MD simulations at the atomic level further reveal that the modulation of WCA results from the change of the interfacial water structures of the droplet under an external electric field. This work reports a new phenomenon of anomalous wetting and sheds light on a comprehensive understanding of water-substrate interactions in the presence of external electric fields, driving further applications[22−25] in areas of microfluidics, electrowetting display, printing technology, etc.

The WCA on a substrate is the key indicator to characterize its wettability.[26] The well-known Young equation is commonly used to describe the WCA formed by the interfacial tensions,

$$\gamma_{LV} \cos \theta_0 = \gamma_{SV} - \gamma_{SL} \tag{1}$$

where θ_0 is the inherent WCA on the solid surface without an external field, and γ_{LV}, γ_{SV}, and γ_{SL}, are the surface tensions between liquid−vapor, solid−vapor, and solid−liquid phases, respectively. When the electric field is applied to the conductive water droplet, the Young equation is modified to the Young−Lippmann equation to describe the change of the contact angle in relation to the electric field (E):

$$\cos \theta = \cos \theta_0 + \frac{\langle \varepsilon \varepsilon_o |\boldsymbol{E}|^2 \rangle D}{2\gamma_{LV}} \tag{2}$$

where ε and D represent the dielectric constant and thickness of the interfacial double layer respectively, and ε_0 is the permittivity of a vacuum. The equation indicates that the electric field usually makes the system more hydrophilic. However, this equation only applies to aqueous electrolytes and seems to fail for deionized water in a strong electric field or droplets with the size below the Debye screening length.[27] It is thus natural to speculate that the morphology of deionized water droplets may depend on the strength and direction of the electric field in a distinct way.

The model system we adopt for the atomic level MD simulations is illustrated in Figure 1a, where a water droplet containing 2165 water molecules is placed on a model hexagonal lattice with the (0001) facet. A simple point charge (SPC/E) water model[28] is used with the water-substrate interaction described by the Lennard−Jones (LJ) potential, $V_{LJ} = 4\varepsilon_{SO}\left[\left(\frac{\sigma_{SO}}{r}\right)^{12} - \left(\frac{\sigma_{SO}}{r}\right)^{6}\right]$, where ε_{SO} and σ_{SO} represent the depth of the potential well and the distance between particles with zero potential energy. For the hydrophobic case, a small value of 0.085 kcal/mol is assigned to ε_{SO} in the LJ potential, which means a small adsorption energy of water molecules on solid. We estimate the liquid−vapor surface tension using the equation $\gamma_{LV} = (E_{slab} - E_{bulk})/2$, where E_{slab} and E_{bulk} are the energy of a slab of water and the same volume of bulk water, under an electric field. We use γ_{LV}^0 to denote the liquid−vapor surface tension in the absence of an electric field, which is estimated to be 12×10^{-2} N/m at 300 K, comparable to the experimental value of 7.2×10^{-2} N/m. As shown in Figure 1b, the estimated relative liquid−vapor surface tension ($\gamma_{LV}/\gamma_{LV}^0$) for a hydrophobic substrate displays a nonlinear growth with the rise of electric field strength E. Applying an electric field of equal strength and opposite directions does not change the total energy of the water slab, so the variation of the average relative surface tension with electric field strength from −1 to 0 V/nm is expected to be essentially symmetric with that from 0 to 1 V/nm. Meanwhile, the relation between the cosine of WCA and field strength E for water droplet on the hydrophobic substrate is shown in Figure 1c, revealing a negatively correlated parabolic relationship. Since γ_{LV} grows nonlinearly with the electric field strength, the cosine of contact angle will decrease with increasing electric field, regardless of the direction in which the electric field is applied along the surface normal direction. It is quite different from the conventional EWOD cases which would follow eq 2. It is worth noting that the response of contact angle to an upward or downward electric field is slightly asymmetric, as also shown in ref 19. This is owing to the existence of the solid−liquid interface. The interaction between water molecules and the substrate imposes a strong constraint on the dipole orientation

https://doi.org/10.1021/acs.jpclett.3c03104
J. Phys. Chem. Lett. 2023, 14, 11735−11741

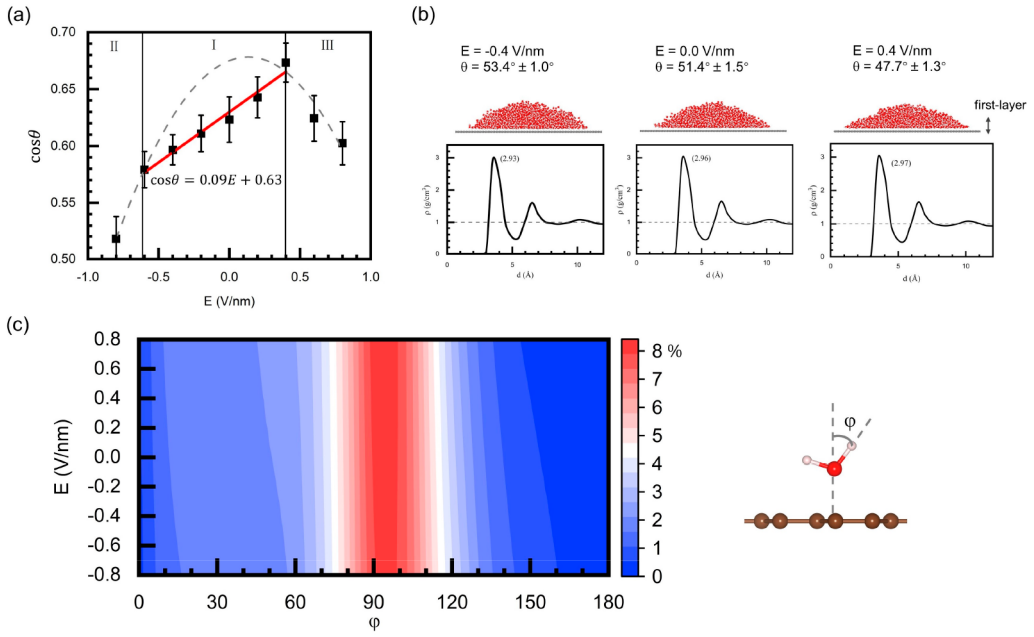

Figure 2. (a) Variation of the cosine of WCA on a hydrophilic substrate with electric field *E*. The gray dashed line shows the quadratic fitting of the data in region II and III. The red line represents the linear fitting of the data in region I. (b) Snapshots of water droplets under different electric fields in region I and the corresponding water density profiles as a function of the distance from the substrate surface along normal direction. (c) Distribution of OH orientation angle φ for the interfacial water molecules in the first layer of the droplet as a function of electric field *E*. Orientation angle φ is defined as the angle between the OH bond and the interfacial normal direction.

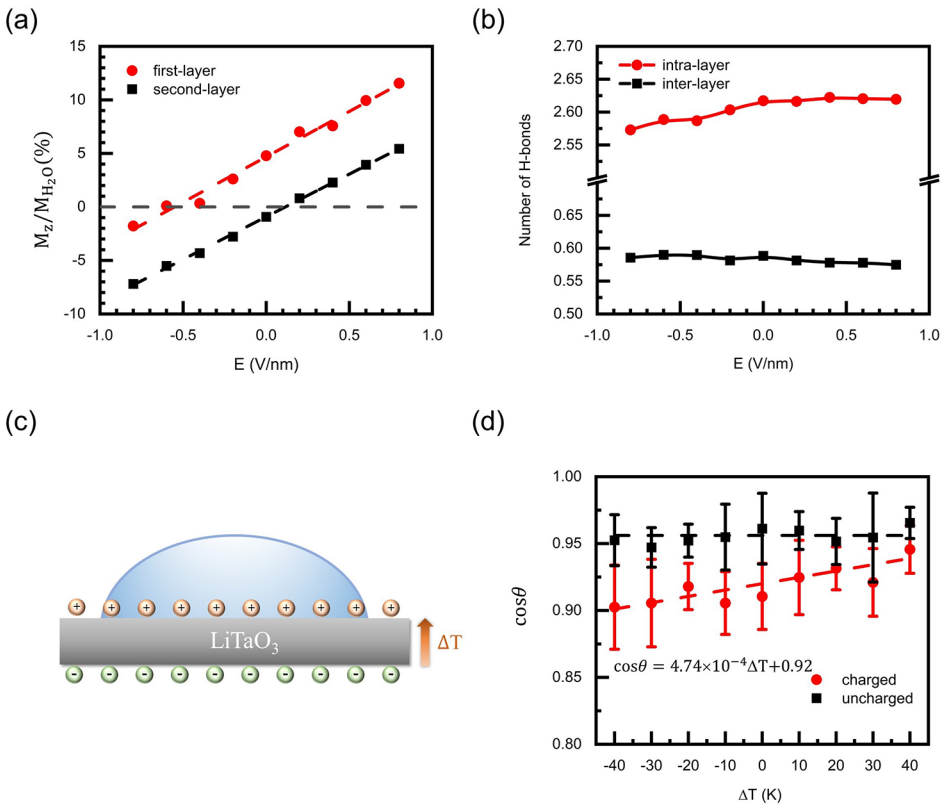

Figure 3. (a) The relative dipole moment of water molecules in the first and second layers of the droplet as a function of the electric field *E*. (b) The average number of hydrogen bonds formed between the interfacial water molecules in the first layer (intralayer bonds) and between molecules in the first and second layers (interlayer bonds), as a function of the electric field *E*. (c) Schematic diagram of the experimental setup for a water droplet deposited on the *z*-cut surface of pyroelectric $LiTaO_3$ crystal, whose surface charge density is modulated by abrupt temperature changes. (d) Variation of the cosine of WCA on $LiTaO_3$ crystals with temperature jump. The red dots and black squares represent the circumstances of charged and uncharged surfaces, respectively.

https://doi.org/10.1021/acs.jpclett.3c03104
J. Phys. Chem. Lett. 2023, 14, 11735−11741

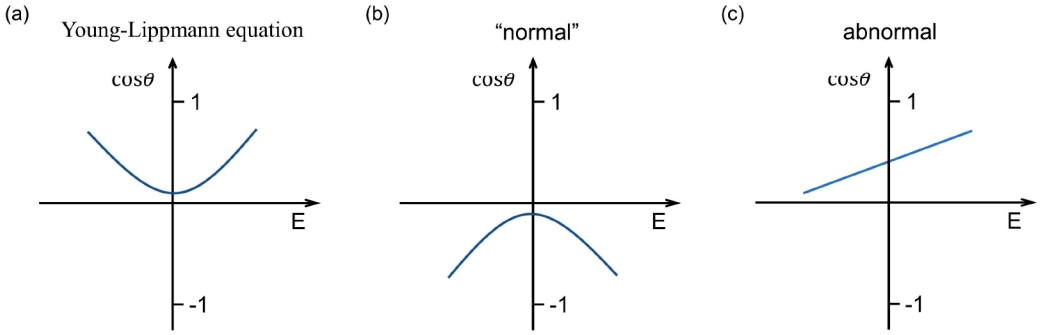

Figure 4. Schematic diagram of water wetting behavior under different conditions: (a) traditional behavior of water under an electric field described by the Young−Lippmann equation; (b) "normal" wetting behavior of deionized water on hydrophobic surfaces, where WCA is governed by liquid−vapor surface tension γ_{LV}, and (c) abnormal wetting behavior of deionized water on hydrophilic surfaces under weak electric fields, where WCA is mainly modulated by the solid−liquid interface.

of the water molecules and eventually results in this asymmetric behavior.

The behavior of WCA on a hydrophilic substrate is shown in Figure 2a. The cosine of WCA exhibits a parabolic relation with E when the field strength is strong enough ($E < -0.6$ V/nm or $E > 0.4$ V/nm), but it displays a linear relation under the weak electric field (region I, -0.6 V/nm $< E < 0.4$ V/nm). The gray dashed line is a quadratic fit to the data of both region II ($E < -0.6$ V/nm) and III ($E > 0.4$ V/nm), and the red solid line is a linear fit to the data of region I. The wetting behavior in region I for the hydrophilic substrate is unconventional. From eq 2, it is expected that the behavior of water droplets on a hydrophilic substrate will be similar to the hydrophobic case, where the cosine of WCA will decrease with the increase of field strength E, but the asymmetric behavior will be more pronounced. However, the results of the MD simulations shown in Figure 2a deviate surprisingly from this trend. Therefore, a reasonable explanation is needed to understand the wettability of water droplets on the hydrophilic substrates in a relatively weak electric field.

We thus explore the molecular structures of water droplets at the water−solid interface at the atomic level. The first row of Figure 2b exhibits the side view snapshots of water droplets under various electric fields in region I from MD simulations, and the second row displays the corresponding density profiles along the normal direction of the substrate. According to the position of first minimum of the density profiles, the water molecules within 5 Å from the substrate surface are defined as the first layer of the droplet, and the rest is referred to as the second water layer. Within region I, the maximum density of the first layer water varies with the electric field, demonstrating a similar trend to the wetting behaviors shown in Figure 2a; i.e., the maximum density of the first layer water increases continuously when the electric field changes from −0.4 to 0.4 V/nm. As the density of water molecules within the first layer increases, the droplet behaves more hydrophilic.

To achieve insight into the structure of interfacial water, the orientations of first-layer water molecules are analyzed and shown in Figure 2c, where the definition of OH orientation angle φ is shown on the left, namely, the angle between the OH bond and the interfacial normal. Distribution of OH orientation angle φ in Figure 2c suggests that as the electric field strength increases from −0.8 V/nm to 0.8 V/nm, the distribution of OH bond orientation is mainly maintained around 96°, but a small fraction of OH bonds tend to align along the normal direction under the electric field and show a linear variation with increasing electric field. This suggests that the interfacial water structure is modulated by the electric field at the microscopic scale.

To reveal the mechanism behind the abnormal behavior of WCA on a hydrophilic substrate in electric fields, we analyze the variation of the relative dipole moment and the number of hydrogen bonds with the electric field strength in the simulations. We define the distribution of the relative dipole moment of water as $\frac{M_z}{N \cdot M_{H_2O}}$, where M_z and M_{H_2O} denote the value of the total dipole moment along the interface normal direction and the dipole moment of single water molecule, respectively, and N is the number of molecules. The responses of water molecules in different layers to the electric field are quite distinct. The relative dipole moments of water molecules in both the first and second layers, as shown in Figure 3a, vary linearly with the electric field E. Notably, the total dipole moment of the first layer of the water droplet shows a hysteresis, changing sign at −0.6 V/nm, which is located on the dividing line between region I and region II. This clearly suggests that the first layer of water droplet is the dominant factor in determining the solid−liquid surface tension γ_{SL}, and the rest possesses the properties of bulk water. For the case of hydrophilic substrates, when the external field E is weak, the surface tension γ_{SL} dominates the change of WCA, while the surface tension γ_{LV} plays only a minor role (as shown in Figure 1b, with a slight increase at small E). Therefore, the linear increase of the dipole moment of the first layer without changing signs leads to the linear change of γ_{SL} and eventually results in an increase of cos θ in region I. As the field strength E increases to region II and III, the influence of the liquid−vapor interface will overwhelm that of the solid−liquid interface, so the wetting behavior of water droplets under large electric fields reverts to a trend similar to that of the hydrophobic substrate.

The characteristics of hydrogen bonds in the droplet are also presented in Figure 3b. The average number of hydrogen bonds formed between the interfacial water molecules in the first layer (i.e., intralayer bonds) and those formed between the molecules in the first and second layers (i.e., interlayer bonds) are reported. The number of intralayer hydrogen bonds increases with rising field strength E and becomes saturated at $E > 0.4$ V/nm. In contrast, the interlayer bonds change slightly and decrease with increasing E. In a gradually increasing electric field, combining the increase in the number of intralayer bonds and the decrease in the number of interlayer

https://doi.org/10.1021/acs.jpclett.3c03104
J. Phys. Chem. Lett. 2023, 14, 11735−11741

bonds, water droplets are prone to remain layered rather than getting higher, which also leads to enhanced hydrophilicity.

In order to verify the anomalous wetting behavior on a hydrophilic substrate under an electric field found in the theoretical simulations, we perform experimental measurements on water droplets deposited on the z-cut surface of pyroelectric $LiTaO_3$ crystal with a controlled temperature,[29] as schematically shown in Figure 3c. The surface charge density is related to the pyroelectric coefficient of the crystal and can be modulated by abrupt temperature changes. Our analysis shows that a large net surface charge of up to 0.1 C/m^2 can be nominally achieved with an abrupt temperature jump $\Delta T = 40$ K, which imposes a strong electric field on water droplets on the surface of $LiTaO_3$ crystal. The correlation between the cosine of WCA on charged or uncharged surfaces and temperature difference is demonstrated in Figure 3d. For the case of uncharged substrates, the cosine of WCA remains constant and independent of substrate temperature jump (black squares) so that the effect of temperature can be excluded. When the substrates are charged, the relationship between $\cos\theta$ and ΔT shows a linear correlation, as indicated by red dots in Figure 3d, with the same trend found in simulations with low external fields, shown in region I of Figure 2a. The values of two data sets (uncharged vs charged) in Figure 3d are not equal at $\Delta T = 0$ K, due to the different sample cleaning histories. However, the crystals in each data set have the same cleaning history to ensure that the trend displayed by each line is reliable.

In contrast to the conventional EWOD cases, where an electric double layer is formed and the WCA decreases with increasing strength of electric field (Figure 4a), the WCA of deionized water droplets behave in the opposite way under a strong electric field where the electric double layer cannot shield the field completely (Figure 4b). More importantly, when the applied field is weak, the water droplet on a hydrophilic substrate shows an anomalous wetting tendency, where the cosine of WCA is linearly related to the electric field value (Figure 4c). This anomaly can be explained by the fact that for a hydrophilic substrate, the solid−liquid interfacial tension is linearly modulated by the electric field and plays a dominant role.

In summary, by combining atomistic simulation and experimental study, we provide a comprehensive picture of the wetting behavior of deionized water under an electric field and gain insight into the functions of an electric field in modulating water wettability at the microscopic level. The new mechanism of electrowetting identified here can be used in a variety of circumstances. For example, we can increase the WCA instead of decreasing it in the traditional EWOD case, which will help in cleaning because one can dissolve contaminants in the hydrophilic case and allow them flow away in the hydrophobic case. In addition, the WCA can be linearly modulated in the abnormal region, which can be designed for microfluid control, since the flow rate is related to the contact angle. We emphasize that substrate surface polarization and screening are not considered here so that the pure effect of electric fields on the wetting behavior of deionized water is investigated. Surface screening and field effects are subjects deserving further study, but they are beyond the scope of this work. We expect our findings may contribute to the design and application of electrowetting and microfluidics, and inspire further exploration of novel physical phenomena in interfacial water under electric fields.

METHODS

Molecular Dynamics Simulations. The model system for MD simulations contains a water droplet of 2165 molecules placed on a model hexagonal lattice with the (0001) facet. The lattice constant of the substrate is 2.46 Å, and the size of the supercell used in the simulations is chosen to be 40 nm × 40 nm × 100 nm to avoid the interactions between periodic images.[30] Periodic boundary conditions are applied in all three dimensions. For simplicity, all atoms of the model substrate are fixed. The water−substrate interaction is modeled by a 12−6 Lennard−Jones potential, $V_{LJ} = 4\varepsilon_{SO}\left[\left(\frac{\sigma_{SO}}{r}\right)^{12} - \left(\frac{\sigma_{SO}}{r}\right)^{6}\right]$, where ε_{SO} represents the depth of the potential well that is set to be 0.085 and 0.145 kcal/mol for the hydrophobic and hydrophilic cases, respectively, and σ_{SO} represents the distance between particles with zero potential energy, which is set to be 0.34 nm for both cases. All the short-range forces are truncated at 1.0 nm and the Particle-Particle-Particle-Mesh Ewald method[31] is used for the summation of long-range Coulomb interactions. A velocity-Verlet integrator with a time step of 1.0 fs is used in the simulations. The system is pre-equilibrated for 7 ns in a constant volume and temperature (NVT) ensemble with a Nosé−Hoover thermostat[32] at 300 K in the absence of an external electric field. Then we apply the electric field and continue the MD simulation for 7 ns. The trajectories of the last 2 ns are used for further analysis. The strength of electric field is set in the range of −0.8 V/nm to 0.8 V/nm to avoid significant shape changes of water droplet deviating from the sphere. WCA is estimated according to Werder's method,[33] with a statistical error of up to ±1.5°. All simulations are carried out using the LAMMPS program,[34] and visualization is implemented by the OVITO package.[35]

To exclude the influence of size effects on our findings, we also performed simulations for larger droplets composed of 11225 water molecules. The results show that the phenomena revealed in our work are independent of the droplet size. Although evaporation of nanodroplet is typically significant due to Kelvin effect and vacuum environment, previous studies have shown that for a nanosized water droplet in an open environment, complete evaporation requires a microsecond time scales,[36] beyond the time scale of our simulations. In addition, we also find during the pre-equilibration of the system at 300 K for 7 ns that the droplet evaporates about 2% of water molecules before reaching evaporation saturation. Therefore, the evaporation effect has a negligible impact on the nanosecond processes we study.

Experimental Procedures. Wetting experiments under the electric field are performed to verify the theoretical predictions. Due to the insulating property of deionized water, an ultrastrong electric field (much stronger than the air breakdown threshold of 0.003 V/nm) is required to obtain significant changes in the water droplet. However, only a weak electric field can be applied in EWOD (otherwise the electrical breakdown happens).[21] To this regard, the pyroelectric $LiTaO_3$ crystals are chosen to obtain an enormous surface charge density[37] (corresponding to a field strength up to 0.02 V/nm in the crystal) via abrupt temperature changes (estimated to be 40 K/s). Water droplets are deposited onto z-cut $LiTaO_3$ crystals (to avoid the abrasion between the bottom surface of crystal and the holder), which is supported by an insulating holder in controlled aerosols.

https://doi.org/10.1021/acs.jpclett.3c03104
J. Phys. Chem. Lett. 2023, 14, 11735−11741

Prior to transfer to the holder, the crystals are rinsed with deionized water and soaked in acetone-isopropyl-alcohol-ethanol-water for two cycles of ultrasonic cleaning, followed by UVO treatment to remove organic impurities. Through heating the holder and transferring the crystals to the holder, net charges accumulate on the crystal surface due to pyroelectric coefficient and temperature change. The $LiTaO_3$ crystal used here has a pyroelectric coefficient of 2.3×10^{-4} C/(m^2·K),[38] which is constant below 100 °C. Because of the finite size effects, the field effect will not be completely screened as in the infinite parallel plate capacitor, which only persist in the vicinity of the substrate. Then 0.5 μL of deionized water, with electric resistivity greater than 18 MΩ·cm, is deposited through the insulating syringe needle within a minute. The diameter of the water droplets is estimated to be several millimeters. The value of WCA is obtained from the first frame when the spherical cap droplet appears on the crystal to avoid the effect of evaporation on shape of droplets. The measurements are performed in a room temperature environment, and the relative humidity is kept below 3%.

AUTHOR INFORMATION

Corresponding Authors

Cui Zhang − *Beijing National Laboratory for Condensed Matter Physics and Institute of Physics, Chinese Academy of Sciences, Beijing 100190, China; Songshan Lake Materials Laboratory, Dongguan 523808, China;* orcid.org/0000-0002-2154-5187; Email: cuizhang@iphy.ac.cn

Haizhong Guo − *Key Laboratory of Material Physics, Ministry of Education, School of Physics and Microelectronics, Zhengzhou University, Zhengzhou 450001, China;* orcid.org/0000-0002-6128-4225; Email: hguo@zzu.edu.cn

Sheng Meng − *Beijing National Laboratory for Condensed Matter Physics and Institute of Physics, Chinese Academy of Sciences, Beijing 100190, China; School of Physical Sciences, University of Chinese Academy of Sciences, Beijing 100049, China; Songshan Lake Materials Laboratory, Dongguan 523808, China;* orcid.org/0000-0002-1553-1432; Email: smeng@iphy.ac.cn

Authors

Qiuhao Xu − *Beijing National Laboratory for Condensed Matter Physics and Institute of Physics, Chinese Academy of Sciences, Beijing 100190, China; School of Physical Sciences, University of Chinese Academy of Sciences, Beijing 100049, China*

Yutian Shen − *Beijing National Laboratory for Condensed Matter Physics and Institute of Physics, Chinese Academy of Sciences, Beijing 100190, China; School of Physical Sciences, University of Chinese Academy of Sciences, Beijing 100049, China*

Runlai Xu − *Beijing National Laboratory for Condensed Matter Physics and Institute of Physics, Chinese Academy of Sciences, Beijing 100190, China*

Qunfang Gu − *Beijing National Laboratory for Condensed Matter Physics and Institute of Physics, Chinese Academy of Sciences, Beijing 100190, China; School of Physical Sciences, University of Chinese Academy of Sciences, Beijing 100049, China*

Complete contact information is available at: https://pubs.acs.org/10.1021/acs.jpclett.3c03104

Author Contributions

#Q.X. and Y.S. contributed equally to this work. C.Z., H.G., and S.M. conceptualized the work. Q.X. and Y.S. performed the ab initio simulations and the experimental measurements. The paper was written by Q.X., C.Z., and S.M. All authors contributed to the discussions and analyses of the data and approved the final version.

Notes

The authors declare no competing financial interest.

ACKNOWLEDGMENTS

We acknowledge financial support from the Ministry of Science and Technology of the People's Republic of China (MOST Grant No. 2021YFA1400503, 2021YFA1400201), the National Natural Science Foundation of China (Grant Nos. 11974400 and 12025407), the CAS Project for Young Scientists in Basic Research YSBR-047 and the "Strategic Priority Research Program B" of the CAS (No. XDB330301).

REFERENCES

(1) Björneholm, O.; Hansen, M. H.; Hodgson, A.; Liu, L.-M.; Limmer, D. T.; Michaelides, A.; Pedevilla, P.; Rossmeisl, J.; Shen, H.-Z.; Tocci, G.; Tyrode, E.; Walz, M. M.; Werner, J.; Bluhm, H. Water at Interfaces. *Chem. Rev.* **2016**, *116* (13), 7698−7726.

(2) Zope, B. N.; Hibbitts, D. D.; Neurock, M.; Davis, R. J. Reactivity of the Gold/Water Interface During Selective Oxidation Catalysis. *Science* **2010**, *330* (6000), 74−78.

(3) Murakami, D.; Jinnai, H.; Takahara, A. Wetting Transition from the Cassie-Baxter State to the Wenzel State on Textured Polymer Surfaces. *Langmuir* **2014**, *30* (8), 2061−2067.

(4) Quéré, D. Wetting and Roughness. *Annu. Rev. Mater. Sci.* **2008**, *38* (1), 71−99.

(5) Lai, Y.-K.; Pan, F.; Xu, C.; Fuchs, H.; Chi, L.-F. In Situ Surface-Modification-Induced Superhydrophobic Patterns with Reversible Wettability and Adhesion. *Adv. Mater.* **2013**, *25* (12), 1682−1686.

(6) Blossey, R. Self-Cleaning Surfaces — Virtual Realities. *Nat. Mater.* **2003**, *2*, 301−306.

(7) Briscoe, W. H.; Titmuss, S.; Tiberg, F.; Thomas, R. K.; McGillivray, D. J.; Klein, J. Boundary Lubrication under Water. *Nature* **2006**, *444* (7116), 191−194.

(8) Kritzer, P. Corrosion in High-Temperature and Supercritical Water and Aqueous Solutions: A Review. *J. Supercrit. Fluids* **2004**, *29* (1−2), 1−29.

(9) Akiya, N.; Savage, P. E. Roles of Water for Chemical Reactions in High-Temperature Water. *Chem. Rev.* **2002**, *102*, 2725−2750.

(10) Bey, R.; Coasne, B.; Picard, C. Probing the Concept of Line Tension Down to the Nanoscale. *J. Chem. Phys.* **2020**, *152*, 094707.

(11) Surblys, D.; Yamaguchi, Y.; Kuroda, K.; Nakajima, T.; Fujimura, H. Analysis on Wetting and Local Dynamic Properties of Single Water Droplet on a Polarized Solid Surface: A Molecular Dynamics Study. *J. Chem. Phys.* **2011**, *135* (1), 014703.

(12) Bistafa, C.; Surblys, D.; Kusudo, H.; Yamaguchi, Y. Water on Hydroxylated Silica Surfaces: Work of Adhesion, Interfacial Entropy, and Droplet Wetting. *J. Chem. Phys.* **2021**, *155* (6), 064703.

(13) Manukyan, G.; Oh, J. M.; van den Ende, D.; Lammertink, R. G. H.; Mugele, F. Electrical Switching of Wetting States on Superhydrophobic Surfaces: A Route towards Reversible Cassie-to-Wenzel Transitions. *Phys. Rev. Lett.* **2011**, *106* (1), 014501.

(14) Acharya, P. V.; Bahadur, V. Fundamental Interfacial Mechanisms underlying Electrofreezing. *Adv. Colloid Interface Sci.* **2018**, *251*, 26−43.

(15) Svishchev, I. M.; Kusalik, P. G. Crystallization of Liquid Water in a Molecular Dynamics Simulation. *Phys. Rev. Lett.* **1994**, *73* (7), 975−978.

(16) Qi, C.-H.; Zhou, B.; Wang, C.-L.; Zheng, Y.-J.; Fang, H.-P. A Nonmonotonic Dependence of the Contact Angles on the Surface

Polarity for a Model Solid Surface. *Phys. Chem. Chem. Phys.* **2017**, *19* (9), 6665−6670.
(17) Yan, J.-Y; Patey, G. N. Heterogeneous Ice Nucleation Induced by Electric Fields. *J. Phys. Chem. Lett.* **2011**, *2* (20), 2555−2559.
(18) Zhu, X.-Y.; Yuan, Q.-Z.; Zhao, Y.-P. Phase Transitions of a Water Overlayer on Charged Graphene: from Electromelting to Electrofreezing. *Nanoscale* **2014**, *6* (10), 5432−5437.
(19) Ren, H.-R.; Zhang, L.-N.; Li, X.-Y.; Li, Y.-F.; Wu, W.-K.; Li, H. Interfacial Structure and Wetting Properties of Water Droplets on Graphene under a Static Electric Field. *Phys. Chem. Chem. Phys.* **2015**, *17* (36), 23460−23467.
(20) Kargar, M.; Lohrasebi, A. Deformation of Water Nano-Droplets on Graphene under the Influence of Constant and Alternative Electric Fields. *Phys. Chem. Chem. Phys.* **2017**, *19* (39), 26833−26838.
(21) Nelson, W. C.; Kim, C. J. Droplet Actuation by Electrowetting-on-Dielectric (EWOD): A Review. *J. Adhes. Sci. Technol.* **2012**, *26* (12−17), 1747−1771.
(22) Watson, A. M.; Cook, A. B.; Tabor, C. E. Electrowetting-Assisted Selective Printing of Liquid Metal. *Adv. Eng. Mater.* **2019**, *21*, 1900397.
(23) Whitesides, G. M. The Origins and the Future of Microfluidics. *Nature* **2006**, *442* (7101), 368−373.
(24) You, H.; Steckl, A. J. Three-Color Electrowetting Display Device for Electronic Paper. *Appl. Phys. Lett.* **2010**, *97*, 023514.
(25) Fotovvati, B.; Namdari, N.; Dehghanghadikolaei, A. On Coating Techniques for Surface Protection: A Review. *J. Manuf. Mater. Process.* **2019**, *3* (1), 28.
(26) Herminghaus, S. Wetting: Introductory Note. *J. Phys.: Condens. Matter* **2005**, *17* (9), S261−S264.
(27) Daub, C. D.; Bratko, D.; Leung, K.; Luzar, A. Electrowetting at the Nanoscale. *J. Phys. Chem. C* **2007**, *111*, 505−509.
(28) Berendsen, H. J. C.; Grigera, J. R.; Straatsma, T. P. The Missing Term in Effective Pair Potentials. *J. Phys. Chem.* **1987**, *91*, 6269−6271.
(29) Johann, F.; Soergel, E. Quantitative Measurement of the Surface Charge Density. *Appl. Phys. Lett.* **2009**, *95*, 233906.
(30) Shelley, J. C. Boundary Condition Effects in Simulations of Water Confined between Planar Walls. *Mol. Phys.* **1996**, *88* (2), 385−398.
(31) Pollock, E. L.; Glosli, J. Comments on P^3M, FMM, and the Ewald Method for Large Periodic Coulombic Systems. *Comput. Phys. Commun.* **1996**, *95* (2−3), 93−110.
(32) Evans, D. J.; Holian, B. L. The Nose-Hoover Thermostat. *J. Chem. Phys.* **1985**, *83*, 4069.
(33) de Ruijter, M. J.; Blake, T. D.; De Coninck, J. Dynamic Wetting Studied by Molecular Modeling Simulations of Droplet Spreading. *Langmuir* **1999**, *15*, 7836−7847.
(34) Plimpton, S. Fast Parallel Algorithms for Short-Range Molecular Dynamics. *J. Comput. Phys.* **1995**, *117* (1), 1−19.
(35) Stukowski, A. Visualization and Analysis of Atomistic Simulation Data with OVITO−The Open Visualization Tool. *Modelling Simul. Mater. Sci. Eng.* **2010**, *18* (1), 015012.
(36) Schlesinger, D.; Sellberg, J. A.; Nilsson, A.; Pettersson, L. G. M. Evaporative Cooling of Microscopic Water Droplets in Vacuo: Molecular Dynamics Simulations and Kinetic Gas Theory. *J. Chem. Phys.* **2016**, *144* (12), 124502.
(37) Parker, G. W. Electric Field outside a Parallel Plate Capacitor. *Am. J. Phys.* **2002**, *70*, 502.
(38) Glass, A. M. Dielectric, Thermal, and Pyroelectric Properties of Ferroelectric $LiTaO_3$. *Phys. Rev.* **1968**, *172* (2), 564−571.

https://doi.org/10.1021/acs.jpclett.3c03104
J. Phys. Chem. Lett. 2023, 14, 11735−11741